Proc. of the 8th International Symposium on Geotechnical Safety and Risk (ISGSR)
Edited by Jinsong Huang, D.V. Griffiths, Shui-Hua Jiang, Anna Giacomini and Richard Kelly

doi: 10.3850/978-981-18-5182-7_14-004-cd

ISGSR 2022

Regional Liquefaction Evaluation Considering the Effect of Effective Friction Angle and Its Spatial Variability

Zhongling Fu[1], Mengfen Shen[2*], Su He[3], Yuming Chen[4] and Mulin Lan[5]

[1]College of Civil and Transportation Engineering, Hohai University, Nanjing, China.
E-mail: 211304030009@hhu.edu.cn
[2]College of Civil Engineering, Zhejiang University of Technology, Hangzhou, China.
*E-mail: mshen@zjut.edu.cn
[3]College of Civil Engineering, Zhejiang University of Technology, Hangzhou, China.
E-mail: 631347044@qq.com
[4]College of Civil and Transportation Engineering, Hohai University, Nanjing, China.
E-mail: ymchenhhu@163.com
[5]College of Civil Engineering, Zhejiang University of Technology, Hangzhou, China.
E-mail: 1149973522@qq.com

Abstract: Spatial variability and uncertainty of soil properties affect the engineering properties of ground. In this work, the effects of effective friction angle and its spatial variability on the regional liquefaction potential were investigated through a case study by nonlinear dynamic numerical simulation. The spatial correlated random fields of effective friction angle evaluated from CPTs data were generated by the conditional sequential Gaussian simulation method coupled with Monte Carlo simulations. The 3D finite element models with uniform and spatial correlated effective friction angle were then respectively built using the finite-difference program FLAC3D. The results show that the accumulation of excess pore pressure can be divided into three phases. The spatial variability of effective friction angle has prominent influence on the regional liquefaction potential.The selection of effective friction angle for uniform model should be careful as it has non-monotonic influence on the regional liquefaction potential of the site.

Keywords: Liquefaction; spatial variability; random field model; effective friction angle; FLAC3D

1 Introduction

Soil liquefaction is a geological disaster caused by earthquake, which will induce ground settlement, sand boiling, building crack and collapse, etc, and thus brings huge loss of life and property. Therefore, accurate evaluation of liquefaction potential of a site provides basis for liquefaction prevention and mitigation.

To assess the soil liquefaction potential, there are generally three approaches, i.e., the simplified method based on in situ test such as standard penetration test, the laboratory method by conducting dynamic triaxial tests, and the numerical simulation method using constitutive model. With properly calibrated constitutive models, the numerical nonlinear dynamic simulation has shown promising results in capturing the dynamic responses of sand, such as excess pore water pressure, settlement, and effect of earthquake history etc. For example, Asgari et al. (2014) conducted a parametric study in FLAC2D to investigate the effects of soil type, structure weight, and the thickness of liquefiable soil layer on the seismic response of the study site. Basu et al. (2019) used empirical and numerical approaches to compare the predictions of post-liquefaction reconsolidation settlement of a spatially variable site.

It has been realized in the recent decades that spatial variability exists in soil parameters, as the soil properties at adjacent locations in the space would have self-correlation. Introducing reliability and geostatistic theories into liquefaction analysis can fully consider the influence of uncertain factors and improve the accuracy of liquefaction potential evaluation. For example, Montgomery & Boulanger (2016) used nonlinear dynamic numerical simulations of infinite slopes to study the effects of spatial variability in penetration resistances on liquefaction-induced settlement and lateral spreading for gently sloping ground, and to develop guidance on selecting representative properties for uniform models. Wang et al. (2021) investigated the liquefaction response considering the spatial variability of the shear modulus by using different values of the coefficient of variation and the horizontal scale of fluctuation. However, only a few works have been attempted to study the effect of the spatial variation of soil property on liquefaction performance under seismic loading in numerical study.

In this study, the effect of effective friction angle and its spatial variability on regional liquefaction potential was explored. A study site with liquefaction observations in 1999 Chi-Chi earthquake was adopted. The random fields of effective friction angle were generated by the conditional sequential Gaussian simulation method

coupled with Monte Carlo simulations. Then the three dimensional models with uniform and random fields of effective friction angle were constructed by finite-difference program FLAC3D for seismic analysis.

2 Site Conditions and Numerical Modeling

2.1 Site location and the cone penetration tests (CPTs)

The site investigated in this study is located in the Lukang district of the Changhua Coastal Industrial Park (CHCIP), Taiwan. Part of the area, with a dimension of 400 m by 200 m, was selected as study site for numerical analysis, as shown in Fig. 1. The geotechnical laboratory tests and site investigation, 27 cone penetration tests (CPTs), were conducted before the 1999 Chi-Chi earthquake. According to the test results, the site mainly consists of silty sands (SM or SP-SM) with thin layers of silts (ML) or silty clays (CL). The study site is susceptible to liquefaction under dynamic loading (Shen et al. 2018).

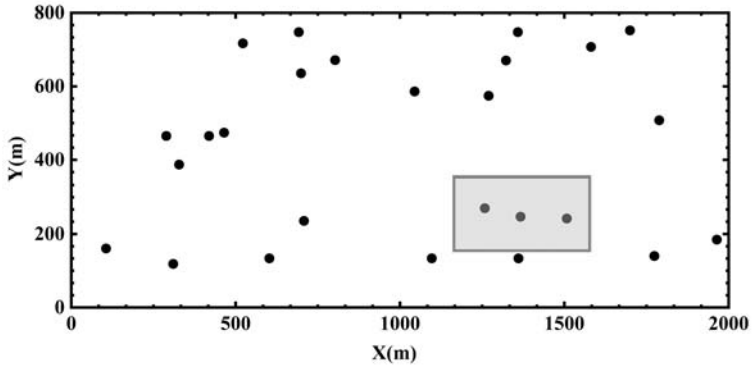

Figure 1. Layout of CPT investigations

2.2 The random field of effective friction angle

The effective friction angle (φ') can be estimated from the cone tip resistance measured in CPTs. The empirical formula proposed by Campanella & Weemees (1990) is adopted in this study:

$$\varphi' = 17.6 + 11\lg\left(\frac{q_c}{\sqrt{\sigma'_{v0}}}\right) \tag{1}$$

where q_c is the cone tip resistance, and σ'_{v0} is the vertical effective stress.

The random fields of φ' was generated by the 2D local soil property approach, in which the random field of φ' was generated layer-by-layer considering the horizontal correlation within the current layer (e.g., Baker and Faber 2008; Juang et al 2017). To generate random field realizations of φ', a conditional sequential Gaussian simulation method coupled with Monte Carlo simulations (Goovaerts 1997) is implemented, which has been extensively used by mining scientists and geostatisticians for natural resource evaluations and spatial prediction of geohazards. Following the conditional sequential Gaussian simulation method, the simulation process could be briefly described as:

$$\left(Z_n \middle| Z_p = z\right) \sim N\left(\Sigma_{np} \cdot \Sigma_{pp}^{-1} \cdot z, \sigma_n^2 - \Sigma_{np} \cdot \Sigma_{pp}^{-1} \cdot \Sigma_{pn}\right) \tag{2}$$

where the subscription *n* and *p* stand for "next" and "previous", respectively; Z_p is the vector for known data; Z_n is the data vector at the unsampled position *n*. Σ is the covariance matrix of adjacent measurements.

The simulated value is randomly drawn from the Gaussian distribution with mean $\Sigma_{np} \cdot \Sigma_{pp}^{-1} \cdot z$ and variance $\sigma_n^2 - \Sigma_{np} \cdot \Sigma_{pp}^{-1} \cdot \Sigma_{pn}$. The simulated data is then added to the known data vector, i.e. Z_p, for the subsequent sequential calculation. The process is repeated with a random path until all the grids at unknown locations are estimated. In this study, the number of Monte Carlo simulation is 300 times as the coefficient of variation (COV) of the simulated fields remains stable.

2.3 Numerical model parameters

The three-dimensional finite-difference ground models with averaged and random fields of effective friction angle were constructed by FLAC3D (Itasca 2017). The analysis domain is 400 m in length, 200 m in width, and 10 m in height, as the gray rectangular shown in Fig.1. The ground water table is 2 m below the ground surface. The grid size is 4m ×4m×1m. The Mohr-Coulomb model was used to simulate the nonlinear soil behavior and the Finn model to simulate the accumulation of pore pressure of soil under a seismic load. The soil parameters in the constitutive model are summarized in Table 1.

Table 1. Properties of soils in uniform model.

Parameters	Symbol	Value
Density（kg/m^3）	)	1600
Porosity	*n*	0.434
Permeability coefficient (cm/s)	*k*	1.00e-3
Bulk modulus (MPa)	*K*	29.41
Shear modulus (MPa)	*G*	11.28
Mean of effective friction angle	)	15.82
Cohesion (kPa)	*c*	8.20

The 1999 Chi-Chi earthquake with magnitude of 7.6 on September 21, 1999 in Taiwan was adopted as the dynamic load applied in the finite-difference model. The epicenter of the Chi-Chi earthquake was located in Chi-Chi Town, Nantou County, Chelongpu fault (120.75 °E, 23.87 °N), with a focal depth of 7.0 km (Lee et al. 2001).

There were four seismic monitoring stations near the Changhua Coastal Industrial Park. The monitoring station at Luojin National Primary School (120.43 °E, 24.06 °N) was the nearest one and thus adopted the seismic wave (shown in Figure 2) applied to the bottom of the numerical model. The X-ACC, Y-ACC, and Z-ACC represents the waveform of seismic acceleration history versus acceleration time in the north to south, east to west, and vertical directions, respectively.

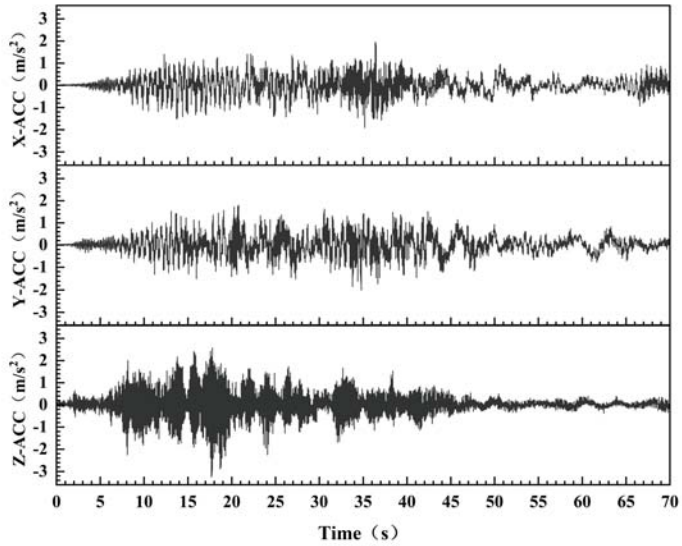

Figure 2. Seismic acceleration history versus time for the 1999 Chi-Chi earthquake.

2.4 Liquefaction criterion

In numerical simulation, the excess pore pressure ratio (PPR) is commonly used to describe liquefaction. In the three-dimensional numerical simulation, the PPR is defined as:

$$\mathrm{PPR} = 1 - \frac{\sigma_1' + \sigma_2' + \sigma_3'}{\sigma_{10}' + \sigma_{20}' + \sigma_{30}'} \tag{3}$$

where σ_{10}', σ_{20}', σ_{30}' are the three principal stresses of the element of the numerical model before dynamic calculation, σ_1', σ_2', σ_3' are the three principal stresses of the element during dynamic calculation (Chen & Xu 2009). The soil element is defined as liquefied if the PPR is greater than 0.75 (Troncoso et al. 1993).

To evaluate the regional liquefaction potential of the study site, liquefaction rate at a site (SLR) is proposed and defined as below:

$$\mathrm{SLR} = \frac{\mathrm{ZN_L}}{\mathrm{ZN_{Total}}} \tag{4}$$

where $\mathrm{ZN_L}$ is the number of element with excess pore pressure ratio greater than 0.75, $\mathrm{ZN_{Total}}$ is the total number of element of the numerical model.

3 Results and Discussions

The φ' estimated from q_c at 27 CPT locations are shown in Figure 3(a). Figure 3(b) is the probability density function of φ' at 27 CPT locations. The φ' fails to follows normal distribution as indicated by the two-sample Kolmogorov-Smirnov test. Thus, the transformation has to be made to transform φ' to the normal distribution. The random fields of φ' were then generated by the conditional sequential Gaussian simulation method coupled with Monte Carlo simulations. One random realization of φ' is shown in Figure 3(c), which serves as the spatial correlated input parameter in the seismic analysis by the FLAC3D.

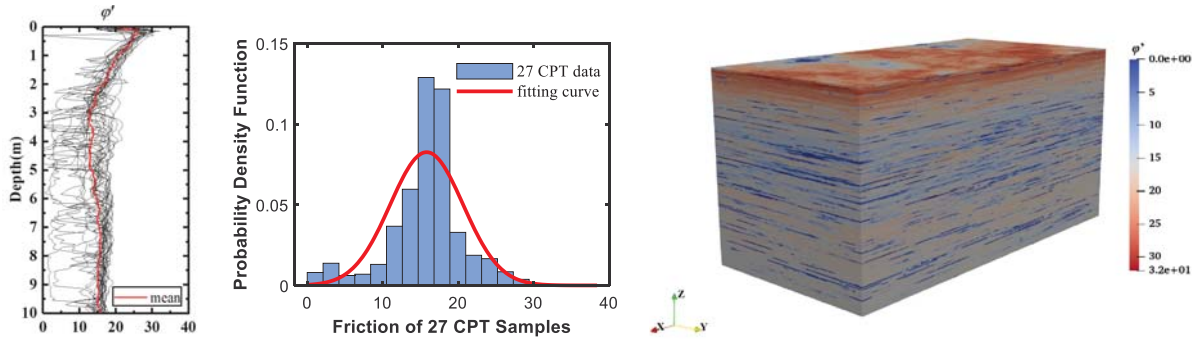

Figure 3. Spatial correlated random field of effective friction angle: (a) cone tip resistance (q_c) of 27 CPTs; (b) effective friction (φ') at test locations; (c) one realization of φ' random field.

The effect of spatial variability of φ' on the SLR of the 3D study field was firstly investigated. The mean SLR value were determined for both uniform φ' field and random field models during the acceleration time of 70s, which is shown in Figure 4(a). The corresponding COV of the random field models is shown in Figure4(b). Under dynamic loading of the Chi-Chi earthquake, three distinct phases can be divided from Figure 4 to capture the accumulation of excess pore pressure, i.e., phase 1: no liquefaction phase with rapid accumulation of excess pore pressure (0-25 s), phase 2: growth phase of liquefaction zone with accumulation of excess pore pressure (25-45 s), and phase 3: fluctuation phase of liquefaction zone without accumulation of excess pore pressure (45-70 s). Similar phenomenon was found in Wang et al. (2021). In phase 1, the pore pressure started to increase rapidly and accumulate. However, the PPR in this phase did not exceed 0.75. In phase 2, the excess pore pressure accumulated to the peak number of liquefaction zone. The liquefaction zones spread continuously in this stage. In phase 3, the SLR fluctuated near the peak number.

In the 300 random field realizations, the COV of SLR in phase 1 was large and decreased rapidly near the end of phase 1. The COV remained closed to zero in phase 2 and 3, indicating the SLR of random field tends to be stable and it is consistent with the soil liquefaction performance. Thus, the SLR in phase 3 can be adopted to determine the regional liquefaction probability of the study site.

Compared the mean values of SLR in phase 3 shown in Figure 6(a), the SLR value of random φ' field model is bigger than that of uniform field. Thus, considering spatial variability of φ' in numerical analysis provides more conservative liquefaction evaluation.

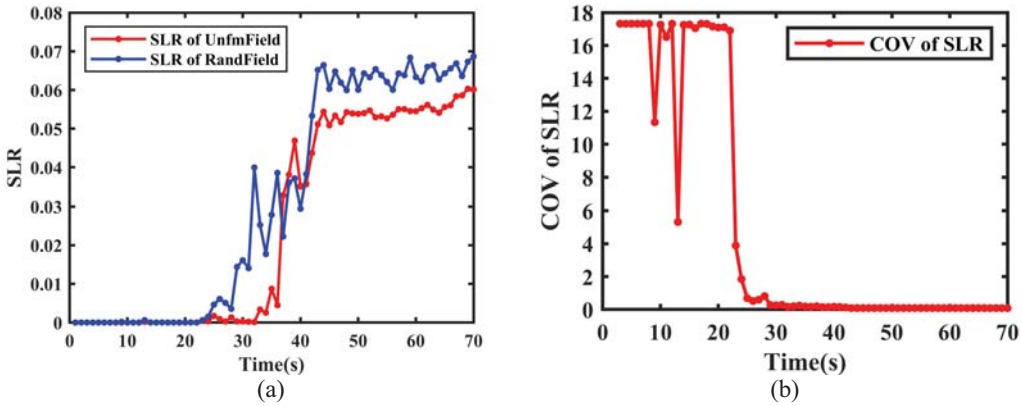

(a) (b)

Figure 4. SLR versus acceleration time: (a) mean of SLR for uniform field and random field models; (b) COV of SLR for random field model.

The average value of φ' at 27 CPT locations is 15.8, which was adopted in the numerical simulation for uniform φ' field. Figure 5(a) shows the PPR map at the end of the dynamic calculation (t=70s) for uniform φ' field at the critical layer, where the PPR value of the elements are maximum. The PPR map with the uniform φ' is relatively smooth and uniform, with a range of PPR from 0.70 to 0.75. There is little liquefaction as most PPR is smaller than 0.75. As a contrast, the PPR map (t=70s) for random φ' field at critical layer is shown in Figure 5(b). One random field realization is adopted to illustrate. The distribution of PPR is discrete with a range of 0.55 to 0.85, many areas are defined as liquefaction in this case. Due to the difference of PPR at adjacent elements, the pore water will flow from the element with high PPR to the element with low PPR. If the outflow is greater than the inflow within the element, the volume of soil will decrease, and vice versa. Compared with the PPR map for uniform φ' field, the random field model can observably reflect the flow of pore water. The spatial variability and uncertainty of φ' has prominent influence on the liquefaction potential of the study site.

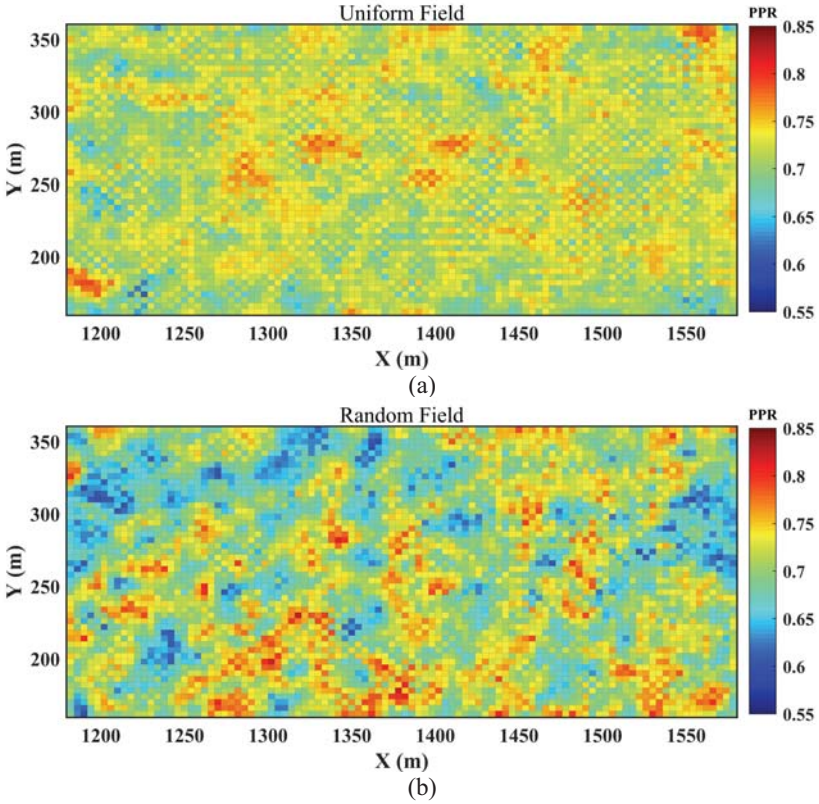

(a)

(b)

Figure 5. PPR map at critical layer with t = 70s for (a) the uniform φ' field; (b) one random φ' field realization.

To explore the influence of φ' on the regional liquefaction potential of the site, the uniform field with different φ' value of 5, 15.8, 20, 25, and 30 were investigated in the numerical simulation. Figure 6(a) shows the SLR at the critical layer versus time. The mean SLR in phase 3 for different uniform φ' field is shown in Figure 6(b). With the increase of the uniform φ' field, the SLR at critical layer increased and then decreased, the SLR reaches peak value when φ' is about 20 degree. Similar phenomena was also observed in Hasheminezhad (2021). Further studies are warranted to explore the inherent reason.

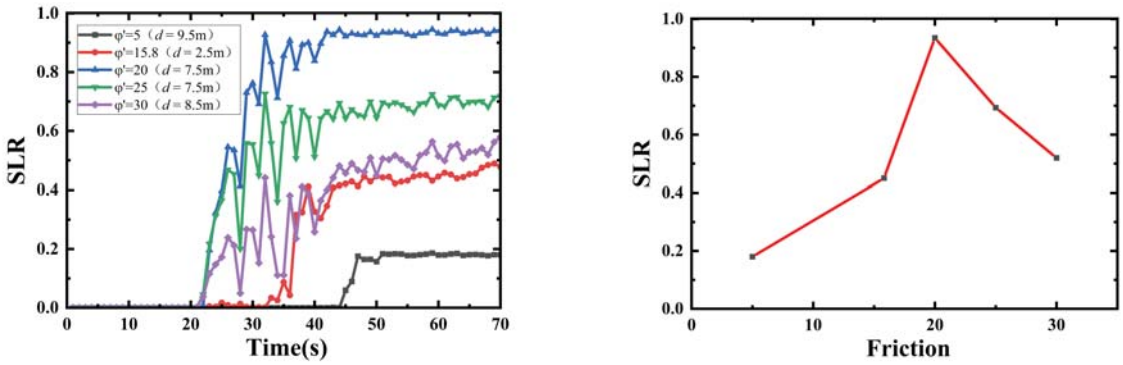

(a) (b)

Figure 6. Effect of effective friction angle on the SLR for uniform field model: (a) SLR at critical depth (*d*) versus acceleration time; (b) SLR versus effective friction angle (*t*=70s).

4 Conclusions

This study aims to investigate the effects of effective friction angle and its spatial variability on the liquefaction potential of a site by the nonlinear dynamic numerical simulations. The the excess pore pressure ratio (PPR) and liquefaction rate at a site (SLR) were adopted to evaluate the liquefaction. It can be concluded:

(1) The accumulation of excess pore pressure of study site can be divided into three distinct phases. The SLR in the third phase can be adopted to determine the regional liquefaction probability of the study site.

(2) Compared with the PPR map for uniform field model of φ', the random field model is discrete and can observably reflect the flow of pore water. The spatial variability of φ' has prominent influence on the regional liquefaction potential of the study site.

(3) With the increase of the effective friction angle, the SLR at the critical liquefaction layer increased and then decreased. The selection of φ' for uniform model should be careful as it has non-monotonic influence on the regional liquefaction potential of the site.

Acknowledgments

The authors would like to acknowledge the financial support from the National Natural Science Foundation of China (42007236) and the Natural Science Foundation of Zhejiang Province, China (Q20D020010).

References

Asgari, A., Golshani, A. , & Bagheri, M. (2014). Numerical evaluation of seismic response of shallow foundation on loose silt and silty sand. *Journal of Earth System Science*, 123(2), 365-379.

Baker, J.W., & Faber, M.H. (2008). Liquefaction risk assessment using geostatistics to account for soil spatial variability. *Journal of Geotechnical and Geoenvironmental Engineering*, 134(1), 14-23.

Basu, D., Montgomery, J., & Stuedlein, A. W. (2019). Comparison of post-liquefaction settlements at a liquefaction test site considering numerical and empirical methods. *In Earthquake Geotechnical Engineering for Protection and Development of Environment and Constructions* (pp. 1370-1377). *CRC Press*.

Campanella, R. G., & Weemees, I. (1990). Development and use of an electrical resistivity cone for groundwater contamination studies. *Canadian Geotechnical Journal*, 27(5), 557-567.

Chen Y.M., Xu D.P. (2009). FLAC/FLAC3D fundamentals and engineering applications. *China Water & Power Press, Beijing, China.*

Goovaerts P (1997) Geostatistics for natural resources evaluation. *Oxford University Press, New York.*

Hasheminezhad, A, & Bahadori, H. (2021). Three dimensional finite difference simulation of liquefaction phenomenon. *International Journal of Geotechnical Engineering*, 15(2), 245-251.

Juang, C. H., Shen, M., Wang, C., Chen, Q. (2018). Random field-based regional liquefaction hazard mapping — data inference and model verification using a synthetic digital soil field. *Bull Eng Geol Environ* 77, 1273 – 1286.

Itasca, F. (2017). Fast Lagrangian analysis of continua in 3-dimensions, version 6.0, manual. *Itasca, Minnesota.*

Lee, D.H., Juang, C.H., Ku, C.S. (2001). Liquefaction performance of soils at the site of a partially completed ground improvement project during the 1999 Chi-Chi earthquake in Taiwan. *Can. Geotech. J.* 38 (6), 1241 – 1253.

Montgomery, J., & Boulanger, R. W. (2017). Effects of spatial variability on liquefaction-induced settlement and lateral spreading. *Journal of Geotechnical and Geoenvironmental Engineering*, 143(1), 04016086.

Shen, M., Martin, J.R., Ku, C.S., & Lu, Y.C. (2018). A case study of the effect of dynamic compaction on liquefaction of reclaimed ground. *Engineering Geology*, 240, 48-61.

Troncoso, J. H., Vergara, A., & Avendaño, A. (1993). Seismic Failure of Barahona Tailings Dam.

Wang, Y., Shu, S., & Wu, Y. (2021). Reliability analysis of soil liquefaction considering spatial variability of soil property. *Journal of Earthquake and Tsunami*, 2250002